Controlling Electron Transfer Dynamics in Donor−Bridge−Acceptor Molecules by Increasing Unpaired Spin Density on the Bridge†

Erin T. Chernick, Qixi Mi, Amy M. Vega, Jenny V. Lockard, Mark A. Ratner,* and Michael R. Wasielewski*

Department of Chemistry and International Institute for Nanotechnology, Northwestern University, Evanston, Illinois 60208-3113

Received: December 19, 2006; In Final Form: January 17, 2007

A *t*-butylphenylnitroxide (BPNO•) stable radical is attached to an electron donor−bridge−acceptor (D−B−A) system having well-defined distances between the components: MeOAn−6ANI−Ph(BPNO•)−NI, where MeOAn = *p*-methoxyaniline, 6ANI = 4-(*N*-piperidinyl)naphthalene-1,8-dicarboximide, Ph = phenyl, and NI = naphthalene-1,8:4,5-bis(dicarboximide). MeOAn−6ANI, BPNO•, and NI are attached to the 1, 3, and 5 positions of the Ph bridge, respectively. Time-resolved optical and EPR spectroscopy show that BPNO• influences the spin dynamics of the photogenerated triradical states ^{2,4}(MeOAn$^{+\bullet}$−6ANI−Ph(BPNO•)−NI$^{-\bullet}$), resulting in slower charge recombination within the triradical, as compared to the corresponding biradical lacking BPNO•. The observed spin−spin exchange interaction between the photogenerated radicals MeOAn$^{+\bullet}$ and NI$^{-\bullet}$ is not altered by the presence of BPNO•. However, the increased spin density on the bridge greatly increases radical pair (RP) intersystem crossing from the photogenerated singlet RP to the triplet RP. Rapid formation of the triplet RP makes it possible to observe a biexponential decay of the total RP population with components of τ = 740 ps (0.75) and 104 ns (0.25). Kinetic modeling shows that the faster decay rate is due to rapid establishment of an equilibrium between the triplet RP and the neutral triplet state resulting from charge recombination, whereas the slower rate monitors recombination of the singlet RP to ground state.

Introduction

The structural and electronic properties of bridge molecules linking electron donors and acceptors within donor−bridge−acceptor (D−B−A) systems determine the rates of electron (or hole) transfer from D to A.[1−24] Single electron-transfer reactions starting from closed-shell precursors are always accompanied by the formation of radical pairs so that spin dynamics often strongly influences the rates and courses of these reactions.[25−27] One way to significantly alter radical pair (RP) spin dynamics is to generate the radical pair in the presence of additional paramagnetic species. Unpaired spins provided by stable free radicals and triplet state molecules have been shown to increase the rate of radical pair intersystem crossing (RP-ISC) between photogenerated singlet and triplet radical pairs.[28−36] For example, we recently demonstrated[37−39] that covalent attachment of 2,2,6,6-tetramethyl-1-piperidinyloxyl (TEMPO) or nitronyl nitroxide (NN•) stable free radicals to rigid D−B−A molecules perturbs their charge recombination rates via an enhanced RP-ISC mechanism similar to that observed for intermolecular systems,[28,30,31] while not altering the spin−spin exchange interaction within the photogenerated RP.

Modulating the degree of spin delocalization from the appended radical onto B is potentially an important means of controlling the charge recombination dynamics through B. For example, the spin density distribution within NN• is localized largely on its two N−O groups and not on the molecule to which NN• is attached[40] so that appending NN• to B within D−B−A does not result in significant spin delocalization onto B itself. We have modified a previously well-characterized D−B−A system, MeOAn−6ANI−Ph−NI, **7**,[41,42] where MeOAn = *p*-methoxyaniline, 6ANI = 4-(*N*-piperidinyl)naphthalene-1,8-dicarboximide, Ph = phenyl, and NI = naphthalene-1,8:4,5-bis(dicarboximide), by attaching a stable NN• to the phenyl bridge molecule to give MeOAn−6ANI−Ph(NN•)−NI, **8**.[38] Studies of both electron transfer and spin dynamics within **8** showed that the presence of the localized NN• radical on the Ph bridge decreased the rate of charge recombination within MeOAn$^{+\bullet}$−6ANI−Ph(NN•)−NI$^{-\bullet}$ in a manner similar to that observed when the localized TEMPO radical was attached to the NI acceptor.

In the work presented here, we have extended these studies by probing the effect of increasing the unpaired spin density on the bridge molecule on the rate of RP-ISC. To accomplish this goal, we appended a *t*-butylphenylnitroxide (BPNO•) radical to the Ph bridge of **7** to produce **6**. The BPNO• radical has significant spin density at the phenyl position para to the nitroxide so that attachment of BPNO• at its para position to another conjugated π-system results in modest spin delocalization from BPNO• to the appended system. For example, it has been demonstrated that attaching alkyl, alkynyl, and porphyrin groups to BPNO• results in delocalization of spin density onto these groups as observed by EPR spectroscopy.[43] In addition, it has been shown that the spin density in these systems delocalizes more readily through π-bonds than σ-bonds.[44] The BPNO• radical is also very robust, making it an appealing choice for incorporation into D−B−A molecules having possible applications to spintronic devices. We report here on the synthesis, electron-transfer reaction rates, and spin dynamics of this system.

† Part of the special issue "Norman Sutin Festschrift".

* To whom correspondence should be addressed. E-mail: m-wasielewski@northwestern.edu.

10.1021/jp068741v CCC: $37.00
Published on Web 02/20/2007

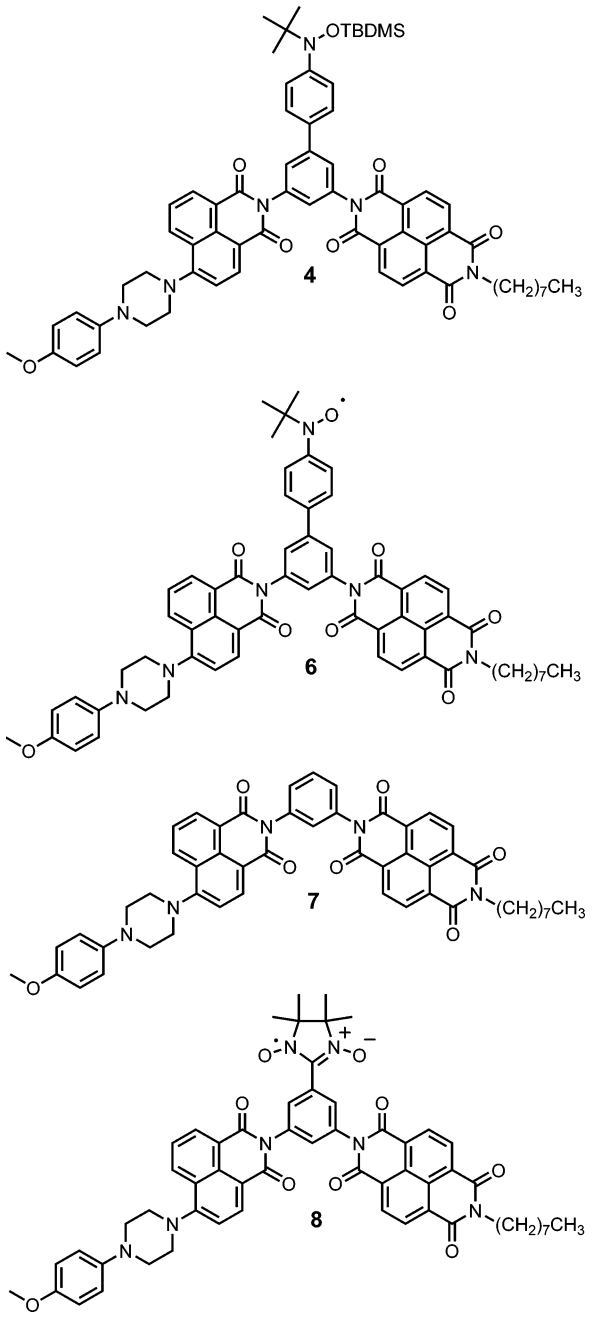

Experimental

The synthesis and characterization of **6** are presented in the Supporting Information.

Cyclic voltammetry measurements were performed in butyronitrile containing 0.1 *M* tetra-*n*-butylammonium perchlorate (TBAP) electrolyte using a CH model 622 electrochemical work station. A 1.0 mm diameter Pt disk electrode, Pt wire counter electrode, and Ag/Ag_xO reference electrode were employed. The ferrocene/ferrocinium couple (Fc/Fc^+, 0.42 V vs SCE) was used as an internal reference for all measurements.

Ground state absorption measurements were made with a Shimadzu (UV-1601) spectrophotometer. Sample solutions were prepared in toluene, transferred to a sealable cuvette, degassed by three freeze−pump−thaw cycles, and then kept under vacuum throughout each spectroscopic run. The optical density of all samples was maintained between 0.2 and 0.5 at 414 nm, ($\epsilon_{6ANI,414}$ nm = 7000 cm^{-1} M^{-1}) for both femtosecond and nanosecond transient absorption spectroscopy.

Femtosecond transient absorption measurements were made using the 414 nm frequency-doubled output from a regeneratively amplified titanium sapphire laser system operating at 2 kHz as the excitation pulse and a white light continuum probe pulse as described earlier.[45] Samples were placed in a 2 mm path length glass cuvette equipped with a vacuum adapter and subjected to five freeze−pump−thaw degassing cycles. The samples were irradiated with 1.0 μJ per pulse focused to a 200 μm spot. The total instrument response time for the pump−probe experiments was 150 fs. Transient absorption kinetics were fit to a sum of exponentials with a Gaussian instrument function using Levenberg−Marquardt least-squares fitting.

Samples for nanosecond transient absorption spectroscopy were placed in a 10 mm path length quartz cuvette equipped with a vacuum adapter and subjected to four freeze−pump−thaw degassing cycles. The samples were excited with 6 ns, 2 mJ, 416 nm laser pulses generated using the frequency-tripled output of a Continuum Precision II 8000 Nd:YAG laser to pump a Continuum Panther OPO. The excitation pulse was focused to a 5 mm diameter spot and matched to the diameter of the probe pulse generated using a xenon flashlamp (EG&G Electro-Optics FX-200). The signal was detected using a photomultiplier tube with high voltage applied to only four dynodes (Hamamatsu R928). The total instrument response time is 8 ns and is determined primarily by the laser pulse duration. The sample cuvette was placed between the poles of a Walker Scientific HV-4W electromagnet powered by a Walker Magnion HS-735 power supply. The field strength was measured by a Lakeshore 450 gaussmeter with a Hall effect probe. Both the electromagnet and the gaussmeter were interfaced with the data collection computer, allowing measurement and control of the magnetic field to $\pm 1 \times 10^{-5}$ T during data acquisition. Due to the length of the sample runs (>3 h), a small amount of sample degradation was observed, resulting in a decrease in the triplet yield at zero field, ΔA ($B = 0$), over the course of the experiments. To compensate for this, the magnetic field was reset to $B = 0$ mT every 3 kinetic traces and ΔA ($B = 0$) was plotted and fit with a linear trendline. These functions were used to calculate the relative triplet yield or RP yield as a function of applied field strength. The relative triplet yield is thus

$$\frac{T}{T_0} = \frac{\Delta A(B)}{\Delta A(B=0)} \tag{1}$$

The results presented are an average of three or more experiments conducted on separate days with freshly prepared samples in freshly distilled ACS grade toluene.

For EPR measurements, toluene solutions of sample (0.2 mM) were loaded into a quartz tube (4 mm o.d. × 2 mm i.d.), and subjected to five freeze−pump−thaw degassing cycles on a vacuum line (10^{-4} mBar). The tubes were then sealed using a hydrogen torch and kept in the dark when not being used. Samples were excited using 416 nm, 1 mJ, 7 ns laser pulses from the H_2-Raman shifted output of a frequency-tripled, Q-switched Nd:YAG laser (Quanta Ray DCR-2).

Steady-state EPR spectra, transient CW EPR spectra, and pulse EPR spectra were measured using a Bruker Elexsys E580 X-band EPR spectrometer with a variable-Q dielectric resonator (Bruker ER 4118X-MS5) at room temperature. Steady-state CW EPR spectra were measured under the conditions of ~0.2 to 2 mW microwave power and ~0.01 to 0.05 mT field modulation at 100 kHz. The g values of the spectra were calibrated with a crystalline 2,2-diphenyl-1-picrylhydrazyl (DPPH) standard (g = 2.0036). Transient CW EPR measurements were carried out

SCHEME 1[a]

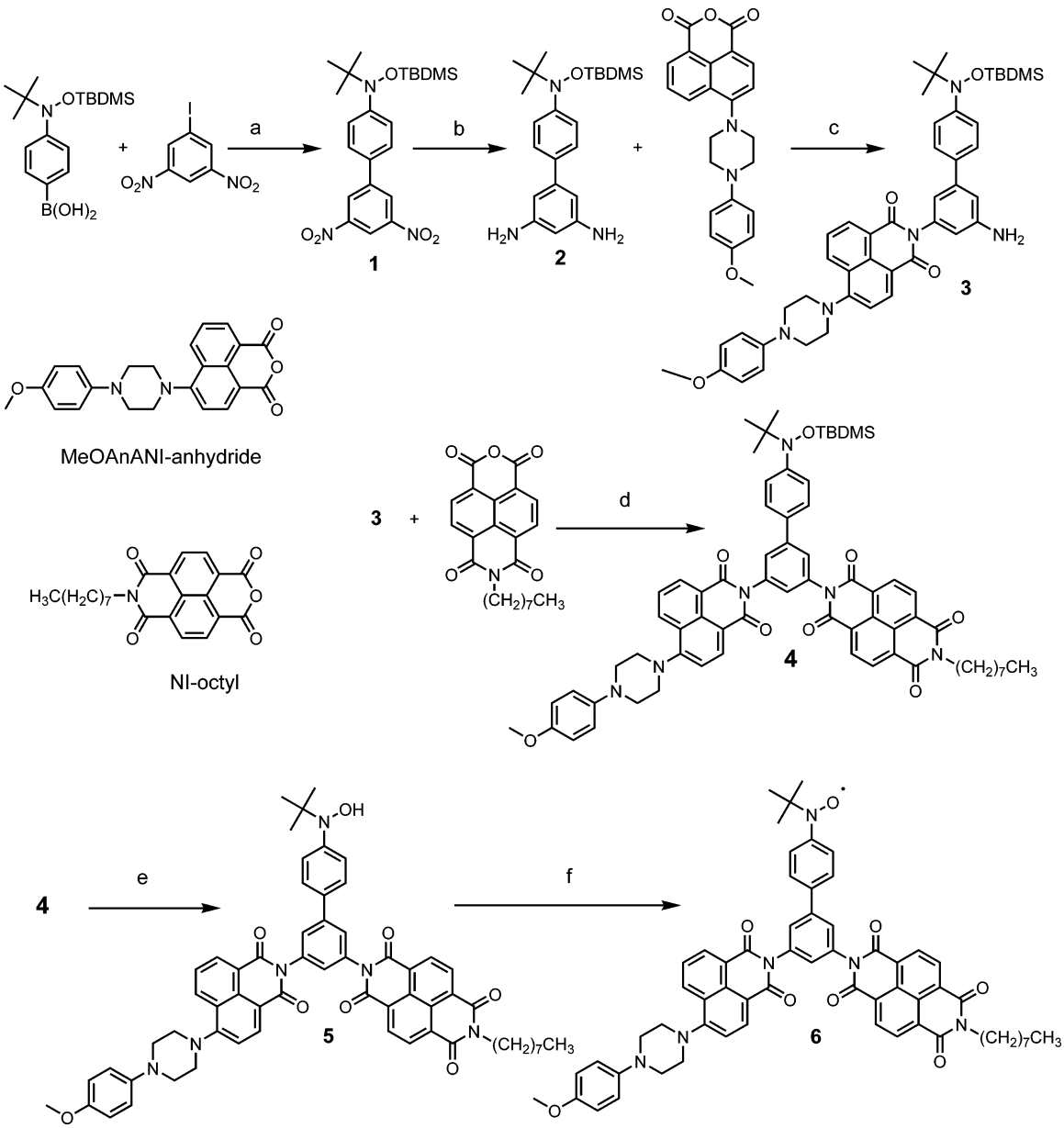

[a] (a) $Pd(PPh_3)_4$, $Na_2CO_{3(aq)}$, toluene, 81%; (b) Pd/C, H_2, EtOH, 71%; (c) MeOAnANI-anhydride, pyridine, reflux, 23%; (d) NI-octylanhydride pyridine, reflux, quantitative; (e) TBAF, THF, −20 °C to room temperature; 28% alcohol, 14% radical; (f) PbO_2, quantitative.

under CW microwave irradiation (typically ~2 to 20 mW) by accumulating kinetic traces of transient magnetization following photoexcitation. The field modulation was disabled to achieve a response time $\tau = Q/\pi\nu \approx 30$ ns,[46] and microwave signals in emission (e) or absorption (a), or both, were detected in both the real and the imaginary channels (quadrature detection). Sweeping the magnetic field gave 2D complex spectra versus time and magnetic field. For each kinetic trace, the signal acquired prior to the laser pulse was subtracted from the data. Kinetic traces recorded off-resonance were considered background signals whose average was subtracted from all kinetic traces. The spectra were subsequently phased into a Lorentzian part and a dispersive part, and the former, also known as the imaginary magnetic susceptibility χ'', is presented.

Results

Synthesis. The complete synthesis for radical **6** is outlined in Scheme 1. Silyl ether-protected 4-(*N*-*t*-butyl-*N*-hydroxylamino)phenylboronic acid was coupled with 3,5-dinitroiodobenzene under Suzuki conditions to yield **1** as a light yellow solid in 81% yield. Compound **1** was then reduced using H_2 over Pd/C to give **2** in 71% yield after purification. Condensation of MeOAnANI-anhydride with **2** gave **3** in a modest 23% yield. The NI-octyl anhydride subunit was condensed with **3** in quantitative yield to give the final TBDMS-protected D−B−A system **4**. Formation of radical **6** was accomplished by deprotecting **4** with TBAF at low temperature to give alcohol **5**. Partial oxidation of the *N*-hydroxyamine in **5** to the nitroxide radical **6** occurs during workup to yield alcohol **5** and radical **6** in 28 and 14% yields, respectively. Oxidation of alcohol **5** using PbO_2 results in quantitative formation of radical **6**.

Steady-State Properties. The photophysical properties of 6ANI, NI and model system **7** have been previously characterized.[41,42,47,48] The ground state optical spectrum of 6ANI exhibits a broad charge transfer (CT) band centered at 390 nm, whereas that of NI exhibits three distinct absorptions due to vibronic

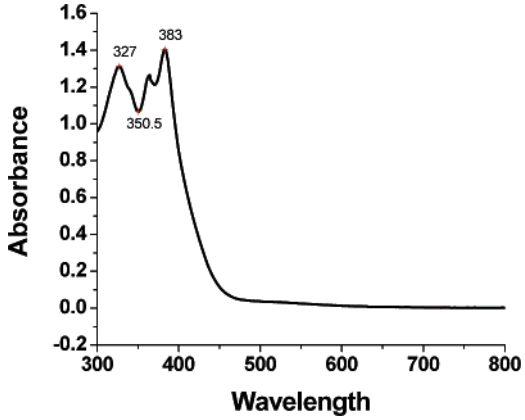

Figure 1. Uv−vis spectrum of **6** in toluene.

structure on the $\pi-\pi^*$ transition at 343, 363, and 382 nm. In radical **6** (MeOAn−6ANI−Ph(BPNO$^\bullet$)−NI), there is an additional absorption band belonging to BPNO$^\bullet$ at 327 nm, which partially overlaps the absorptions of both 6ANI and NI (Figure 1). The redox potentials of model system **7** have been described in detail elsewhere.[41,47] Briefly, the first oxidation potential of ANI occurs at 1.22 V, and the first reduction potential of NI is −0.53 V. These redox potentials do not differ significantly in MeOAn−6ANI−Ph(BPNO$^\bullet$)−NI. However, the presence of the BPNO$^\bullet$ radical results in an additional reversible one-electron oxidation at 0.71 V vs SCE, which is very similar to other *t*-butylphenylnitroxide radicals.[49]

The energy levels of the RPs within **7** have been calculated using the experimental redox potentials and are reported elsewhere.[41] It is assumed that there are no significant changes in the RP energy levels in either **4** or **6**. Thus, the energy level diagram displayed in Figure 2 is the same for **4**, **6**, and **7**.

Transient Absorption Spectroscopy. Photoexcitation of **4** with a 414 nm, 150 fs laser pulse produces ^{1*}6ANI, leading to the reaction MeOAn−^{1*}6ANI−Ph(BPNOR)−NI → MeOAn$^{+\bullet}$-6ANI$^{-\bullet}$−Ph(BPNOR)−NI with a time constant $\tau_{CS1} = 4.0$ ps, as indicated by the formation of an absorption band (shoulder) due to MeOAn$^{+\bullet}$ at 520 nm, where BPNOR is the protected BPNO$^\bullet$ radical. The subsequent reaction, MeOAn$^{+\bullet}$-6ANI$^{-\bullet}$−Ph(BPNOR)−NI → MeOAn$^{+\bullet}$-6ANI−Ph(BPNOR)−NI$^{-\bullet}$ is indicated by the appearance of the absorption features characteristic of NI$^{-\bullet}$ at 480 and 610 nm with $\tau_{CS2} = 40$ ps. Radical **6** has similar charge separation rates: MeOAn−^{1*}6ANI−Ph(BPNO$^\bullet$)−NI → MeOAn$^{+\bullet}$-6ANI$^{-\bullet}$−Ph(BPNO$^\bullet$)−NI with a time constant $\tau_{CS1} = 3.5$ ps and secondary charge-transfer MeOAn$^{+\bullet}$-6ANI$^{-\bullet}$−Ph(BPNO$^\bullet$)−NI → MeOAn$^{+\bullet}$-6ANI−Ph(BPNO$^\bullet$)−NI$^{-\bullet}$ with $\tau_{CS2} = 40$ ps. The femtosecond transient absorption spectra of **6** in toluene are shown in Figure 3. The nanosecond transient absorption spectra for **4** and **6** (Figure 4) show bands at 480 and 610 nm characteristic of NI$^{-\bullet}$, as well as a shoulder at 520 nm due to MeOAn$^{+\bullet}$. The decay of NI$^{-\bullet}$ measured by the disappearance of the NI$^{-\bullet}$ absorption feature at 480 nm occurs with a monoexponential time constant of $\tau_{CR} = 89$ ns for model system **4**, whereas the decay of NI$^{-\bullet}$ for radical **6** is biexponential with time constants of $\tau_{CR1} = 740$ ps (0.75) and $\tau_{CR2} = 104$ ns (0.25). The rapid decay component of NI$^{-\bullet}$ in **6** is shown in the inset to Figure 3, whereas its long decay components of **4** and **6** are shown in the insets to Figure 4. Charge separation (CS) and recombination (CR) rates of all compounds are summarized in Table 1.

Magnetic Field Effect Measurements. The magnetic field effect (MFE) on the rate and yield of RP recombination directly reveals the magnitude of electron spin−spin exchange interaction, 2*J*, between the spins within the RP, which is proportional to the square of the donor−acceptor superexchange coupling, V_{DA}.[19,50−52] The details of the RP-ISC mechanism and the theory behind the MFE have been researched extensively[53−56] and applied to many donor−acceptor systems,[19,41,57−63] including biological[54,64−67] systems. Photoexcitation of compound **4**, which lacks the BPNO$^\bullet$ radical, initially produces the singlet RP, which undergoes electron−nuclear hyperfine coupling-induced RP-ISC to produce the triplet RP, ^{1}(MeOAn$^{+\bullet}$-6ANI−Ph(BPNOR)−NI$^{-\bullet}$) → ^{3}(MeOAn$^{+\bullet}$-6ANI−Ph(BPNOR)−NI$^{-\bullet}$). The subsequent charge recombination process is spin-selective, and the singlet RP recombines to the singlet ground state, whereas the triplet RP recombines to yield the neutral local triplet MeOAn−6ANI−Ph(BPNOR)−^{3*}NI. Application of a static magnetic field splits the RP triplet levels and modifies the rate of RP-ISC. When the Zeeman splitting of the triplet RP levels equals the intrinsic singlet−triplet splitting, 2*J*, of the RP, the rate of RP-ISC is maximized, which leads to a maximum in triplet RP production and, therefore, a maximum in neutral local triplet production upon charge recombination. By monitoring the yield of the neutral triplet charge recombination product as a function of applied magnetic field, the magnitude of the magnetic superexchange interaction, *2J*, can be measured directly.

The same two rapid, nonadiabatic charge separation steps occur in radical **6** as described above for **4**, even though the initial state in **6** is formally a doublet. Figure 5 shows the MFE on the yield of MeOAn−6ANI−Ph(BPNO$^\bullet$)−^{3*}NI and MeOAn−6ANI−Ph(BPNOR)−^{3*}NI resulting from charge recombination. The data show two clear resonances for both **6** and **4** at 1.5 ± 0.5 mT and 15 ± 1 mT, respectively, which indicates that the presence of the BPNO$^\bullet$ radical on the bridge does not perturb the magnitude of the spin−spin exchange interaction between the MeOAn$^{+\bullet}$ and NI$^{-\bullet}$ radicals. The presence of two resonances in the MFE plots in Figure 5 is due to two distinct conformations about the piperazine ring that result in two slightly different RP distances, as discussed previously.[41]

EPR Spectroscopy. The steady-state EPR spectrum of **6** displayed in Figure 6 consists of 21 hyperfine lines centered at $g = 2.0057$ due to the nitrogen of BPNO$^\bullet$ having $|a_N| = 1.18$ mT, and the four protons on the phenyl ring with $|a_H| = 0.21$ mT for the two protons ortho to the nitroxide, and $|a_H| = 0.09$ mT for the two protons meta to the nitroxide. Further hyperfine coupling to protons in the bridge phenyl ring is unresolved but results in line-broadening of the resonances to 0.06 mT from the 0.03 mT line width of the para *t*-butyl derivative of BPNO$^\bullet$.[43] This suggests that the two Ph bridge protons ortho to the point of attachment of BPNO$^\bullet$ are contributing hyperfine splittings of ∼0.015 mT to the observed line width.

Time-resolved EPR (TREPR) spectra (i.e., pulsed laser excitation, CW microwaves) of model compound **4** and radical **6** in toluene at 295 K were measured around $g \approx 2$, the region where RPs and stable radicals are observed. Immediately after laser excitation, both **4** and **6** exhibit an intense photogenerated RP signal with an *emission*, *absorption* (e, a) polarization pattern (Figure 7) centered at $g = 2.0033$, similar to the *g* values of MeOAn$^{\bullet+}$ and NI$^{\bullet-}$.[42] These spin-polarized RP spectra are similar to those observed previously for model compound **7**. At room temperature in fluid solution, molecular tumbling renders the EPR spectra of triplet states broad and structureless[68] and most often undetectable.

Discussion

Energetics and Electron-Transfer Dynamics. The data in Table 1 show that the time constants for both charge-separation

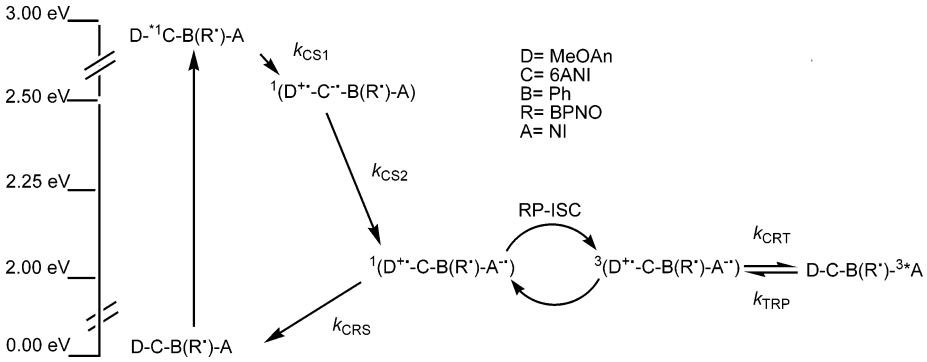

Figure 2. Energy level diagram and electron-transfer pathway representative for compounds **4**, **6**, and **7**.

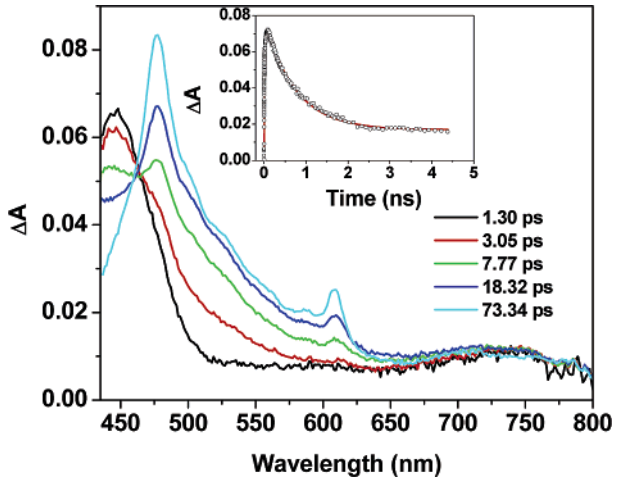

Figure 3. Femtosecond transient absorption spectra of **6** in toluene obtained at the indicated times following a 414 nm, 150 fs laser pulse. Insert: a kinetic trace obtained at 482 nm.

steps in **4**, **6**, and **7** are very similar. Therefore, substitution of the Ph bridge with the protected BPNO• radical or the BPNO• radical itself does not influence the charge separation process. This is reasonable and expected, given that these CS rates are much faster than RP-ISC and thus should not be influenced by the presence of the third spin.[53,55,69−72] Photoinitiated two-step CS within **6** rapidly produces the triradical ^{2}(MeOAn$^{+\bullet}$−6ANI−Ph(BPNO•)−NI$^{-\bullet}$) having an overall doublet spin configuration. Charge recombination within ^{2}(MeOAn$^{+\bullet}$−6ANI−Ph(BPNO•)−NI$^{-\bullet}$) produces the doublet ground state ^{2}(MeOAn−6ANI−Ph(BPNO•)−NI) (k_{CRS}) (Figure 2) whereas RP-ISC leads to a triradical having a pair of doublet states and a quartet state: ^{2,4}(MeOAn$^{+\bullet}$−6ANI−Ph(BPNO•)−NI$^{-\bullet}$). Charge recombination within the triradical (k_{CRT}) produces the neutral doublet and quartet states ^{2,4}(MeOAn−6ANI−Ph(BPNO•)−^{3*}NI). Note that in this case, two unpaired electrons reside on ^{3*}NI so that this species is formally a triplet excited state that can be observed optically.

The free energy of the CR process ^{2,4}(MeOAn$^{+\bullet}$−6ANI−Ph(BPNO•)−NI$^{-\bullet}$) → ^{2,4}(MeOAn−6ANI−Ph(BPNO•)−^{3*}NI) in **6** is ∼0.06 eV so that an equilibrium between these states is established.[73] The observed lifetime of triradical ^{2,4}(MeOAn$^{+\bullet}$−6ANI−Ph(BPNO•)−NI$^{-\bullet}$) differs significantly both from model compounds **4** and **7** not containing the third spin and from radical **8** having a localized NN• radical attached to the Ph bridge (Table 1). The decay of NI$^{-\bullet}$ in **6** is biexponential, with τ_{CR1} = 740 ps (0.75) and τ_{CR2} = 104 ns (0.25), whereas data obtained previously on radical **8** and model compounds **4** and **7** exhibit monoexponential decays of NI$^{-\bullet}$ with τ_{CR} = 101, 89, and 73 ns, respectively.[41] At modest magnetic fields, RP-ISC between singlet and triplet RPs usually occurs via the hyperfine mechanism with a rate of ∼10^{8} s^{-1};[55,56,74] however, an appended stable free radical creates a strong local magnetic field that accelerates RP-ISC, resulting in rapid population of the triplet RP. This mechanism has been termed spin catalysis or enhanced radical pair intersystem crossing (EISC).[29,31,35,75] Given that the triradical in **6** is in equilibrium with its neutral triplet recombination product ^{2,4}(MeOAn−6ANI−Ph(BPNO•)−^{3*}NI), EISC driven by the presence of BPNO• in **6** shifts the population toward the triplet RP, which presents a bottleneck that slows overall CR decay due to the fact that ^{2,4}(MeOAn−6ANI−Ph(BPNO•)−^{3*}NI) is slightly higher in energy than ^{2,4}(MeOAn$^{+\bullet}$−6ANI−Ph(BPNO•)−NI$^{-\bullet}$). This is observed in radical **8**, for which τ_{CR} = 101 ns, whereas for model system **7**, it is τ_{CR} = 73 ns.

The energy levels for **6** are similar to those of **4**, **7**, and **8** so that the BPNO• radical should influence the charge recombination process in **6** in a manner similar to that of NN• in **8**. However, the leakage of spin density onto the phenyl bridge from BPNO• in **6** is greater than that from NN• in **8** so that the spin−spin exchange interaction between the oxidized donor and the radical, $2J_{DR}$, as well as that between the reduced acceptor and the radical, $2J_{RA}$, should be larger for **6** than for **8**. This increased interaction should greatly increase the rate of RP-ISC in **6** so that RP-ISC is no longer rate-limiting, and the kinetics of the rapid equilibrium between ^{2,4}(MeOAn$^{+\bullet}$−6ANI−Ph(BPNO•)−NI$^{-\bullet}$) and ^{2,4}(MeOAn−6ANI−Ph(BPNO•)−^{3*}NI) can be observed directly by transient optical absorption spectroscopy.

Formation of the initial singlet radical pair is followed by coherent evolution of the spin system into a mixed state having both singlet and triplet character. In the absence of spin lattice relaxation, which occurs on a microsecond time scale, this mixed state oscillates between singlet and triplet spin configurations. This intrinsically quantum mechanical process was modeled using a simple equilibrium between singlet and triplet populations occurring with equal rates, k_{ST} and k_{TS}. Two spin-selective charge recombination processes deplete the RP population. The singlet RP recombines to ground state with k_{CRS}, whereas the triplet radical pair recombines to yield the lowest energy neutral triplet state centered on NI with k_{CRT}. Since the triplet RP and the neutral triplet recombination product are very close in energy, an equilibrium occurs between these states so that ^{3*}NI regenerates the triplet RP with k_{TRP}. We have observed this equilibrium directly in model system **7** using TREPR at low temperatures, where k_{CRT} and k_{TRP} are substantially slower.[42] Simulation of the experimental data using the kinetic model in Figure 8 requires both an enhanced RP-ISC rate between the singlet and triplet RPs and the establishment of a rapid equilibrium between the triplet RP and the neutral triplet recombination product. As mentioned above, for model systems

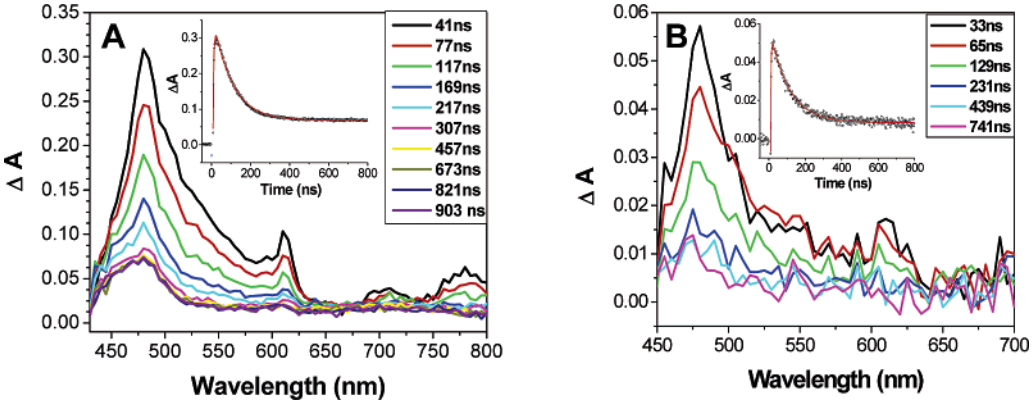

Figure 4. Nanosecond transient absorption spectra of **4** (A) and radical **6** (B) in toluene. The insets show the transient absorption kinetic traces obtained at 480 nm.

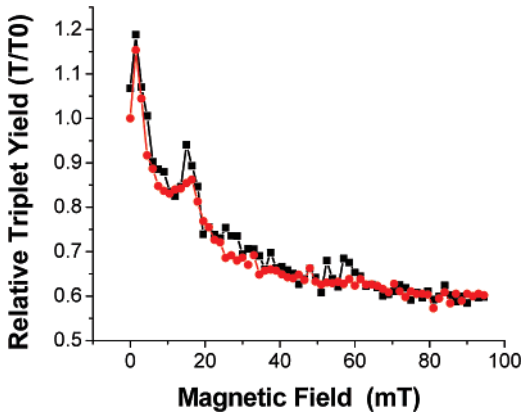

Figure 5. Relative triplet yield of **4** (black) and **6** (red) in toluene as a function of magnetic field strength.

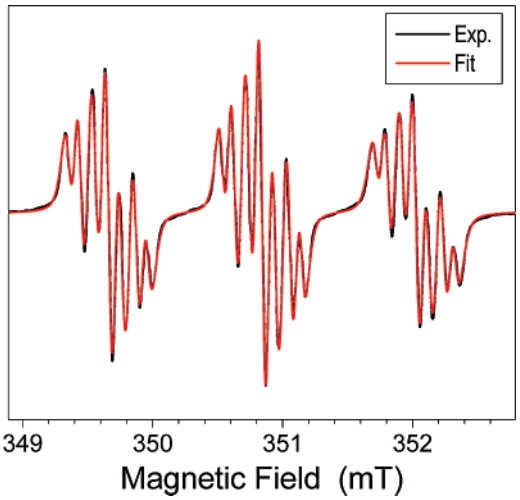

Figure 6. EPR spectrum of **6** in toluene. Shown in an overlay is the experimental (black line) spectrum and the simulated fit (red line).

4 and **7**, as well as for weakly coupled radical pairs in general, $k_{ST} = k_{TS} \sim 10^8$ s^{-1}.[55,56,74] However, to model the experimental kinetic data for **6**, it is necessary to set $k_{ST} = k_{TS} = 10^{10}$ s^{-1}, whereas $k_{CRT} = 2.4 \times 10^9$ s^{-1}, $k_{TRP} = 4 \times 10^8$ s^{-1}, and $k_{CRS} = 1 \times 10^7$ s^{-1}. Using these rate constants, the model illustrated in Figure 8 predicts a biexponential time constant for NI$^{-\bullet}$ decay of $\tau_{CR1} = 688$ ps (0.75) and $\tau_{CR2} = 100$ ns (0.25). These time constants compare favorably with the experimental time constants of $\tau_{CR1} = 740$ ps (0.75) and $\tau_{CR2} = 104$ ns (0.25) (Figure 9). If the RP-ISC rate is reduced to $\leq 10^8$ s^{-1}, the fast component of the biexponential decay is essentially eliminated.

TABLE 1: Summary of Charge Separation and Recombination Time Constants.

compd	τ_{CS1} (ps)	τ_{CS2} (ps)	τ_{CR1} (ps)	τ_{CR2} (ns)
4	4 ± 0.5	40 ± 4		89 ± 2
6	3.5 ± 0.5	31 ± 3	740 ± 70 (0.75)	104 ± 2 (0.25)
7	8.0 ± 1	40 ± 4		73 ± 7
8	11 ± 1	31 ± 3		101 ± 10

Electron Spin−Spin Exchange Interactions in the Photogenerated Triradical. Following photoexcitation, the triradical MeOAn$^{+\bullet}$−6ANI−Ph(BPNO$^{\bullet}$)−NI$^{-\bullet}$ has three pairs of exchange interactions, $2J_{DA}$, $2J_{DR}$, and $2J_{RA}$, where D = MeOAn$^{+\bullet}$, R = BPNO$^{\bullet}$, and A = NI$^{-\bullet}$. The MFE data presented in Figure 5 show that the dominant value of $2J_{DA} = 1.5$ mT and is comparable to that of MeOAn$^{+\bullet}$−6ANI−Ph(BPNOR)−NI$^{-\bullet}$ for reference molecule **4**. The relatively small value of $2J_{DA}$ is consistent with the 20 Å through-bond distance between MeOAn$^{+\bullet}$ and NI$^{-\bullet}$, as has been observed for several related molecules.[41,61,76] Since $2J$ depends exponentially on spin−spin distance,[53] the value of $2J_{RA}$ is expected to be much larger. In earlier work, we estimated that $2J_{RA}$ for the MeOAn$^{+\bullet}$−6ANI−Ph(NN$^{\bullet}$)−NI$^{-\bullet}$ triradical photogenerated from **8** is ≈ 1 T[38] so that increasing the spin density on the Ph bridge in MeOAn$^{+\bullet}$−6ANI−Ph(BPNO$^{\bullet}$)−NI$^{-\bullet}$ should make this value even larger. Last, the exchange coupling between MeOAn$^{+\bullet}$ and NN$^{\bullet}$, $2J_{DR}$, was assumed to be small for MeOAn$^{+\bullet}$−6ANI−Ph(NN$^{\bullet}$)−NI$^{-\bullet}$, perhaps on the same order as $2J_{DA}$, since the two radicals have nearly the same number of bonds (and distance) between them as do MeOAn$^{+\bullet}$ and NI$^{-\bullet}$. However, in the MeOAn$^{+\bullet}$−6ANI−Ph(BPNO$^{\bullet}$)−NI$^{-\bullet}$ triradical, the increased spin density within the Ph bridge should increase $2J_{DR}$ somewhat.

We have previously described how these exchange interactions remix the spin manifold into two doublet states and a quartet state (Figure 10).[38,39] The state Q_1 is the quartet state in which all three spins are parallel, whereas D_1' is the doublet state in which the spins on NI$^{-\bullet}$ and BPNO$^{\bullet}$ are parallel, and D_1 is the other doublet state. Because both D_1' and Q_1 possess parallel NI$^{-\bullet}$ and BPNO$^{\bullet}$ spins, their energy levels are close to each other, but are far removed from D_1, due to the magnitude of $2J_{RA}$. The small energy gap between D_1' and Q_1 at zero field, denoted Δ_{DQ}, can be calculated using a complicated expression depending on all three exchange interactions[31] and turns out to be comparable to $2J_{DA}$.

Using this model, the well-known S−T_0 mixing mechanism[41,74,77,78] of RP-ISC directly translates into D_1'-Q_1 mixing for the triradical so that TREPR spectra with the same polarization pattern should be observed.[38,39] This is a consequence of the fact that the two Zeeman sublevels of D_1' are split

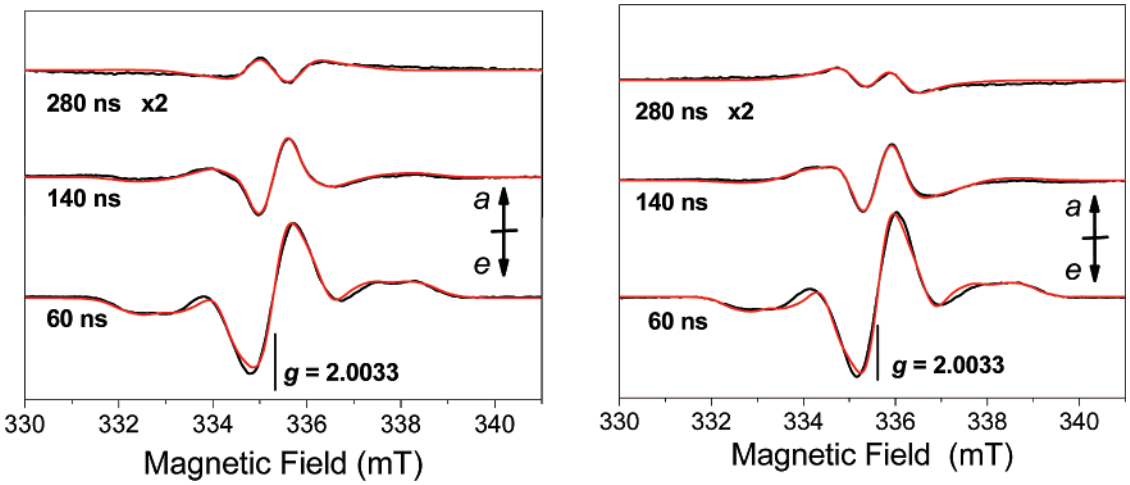

Figure 7. TREPR spectra at the indicated times following a 1.5 mJ, 416 nm, 7 ns laser flash (black traces). Simulations of the spectra (red traces). Left: model compound **4**. Right: radical **6**.

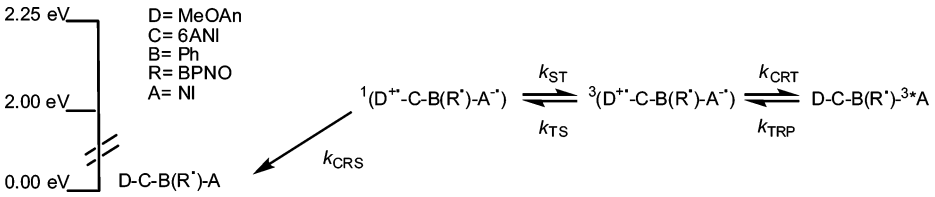

Figure 8. Kinetic model for charge recombination following RP-ISC for **6**.

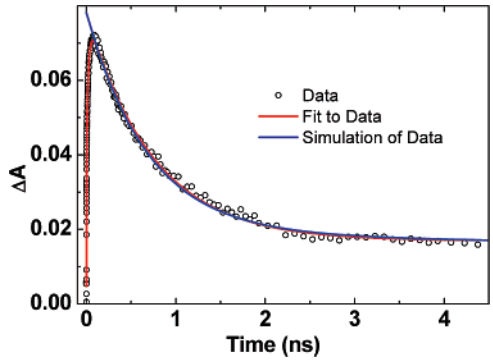

Figure 9. Kinetic simulation for the decay of $NI^{\bullet-}$ in compound **6** using the charge-transfer pathway in Figure 8 and the rate constants discussed in the text.

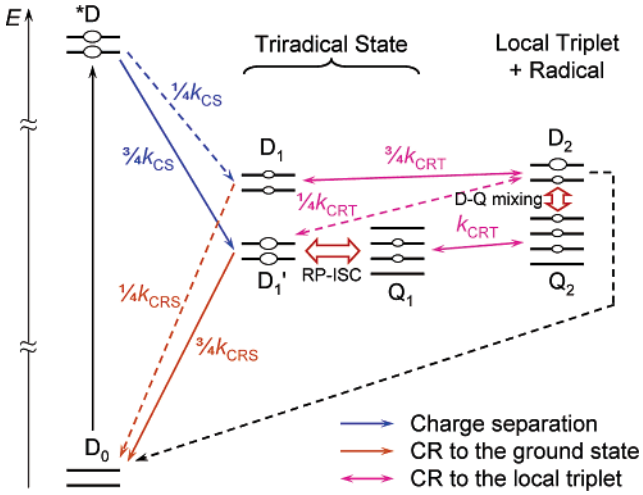

Figure 10. Energy level diagram showing the spin manifolds of **6** after charge separation and charge recombination, in a magnetic field of ~0.35 T. Blue arrows denote charge separation forming the triradical state; orange arrows, charge recombination to the ground doublet state; and magenta arrows, reversible D−D and Q−Q charge recombination steps leading to the local triplet $^{3*}NI$, which is nearly isoenergetic with the RP state in toluene (see text). D_1, D_1', and Q_1 form a complete spin basis set of the triradical state. Dash lines mean less probable transitions. Red double arrows stand for processes that mix certain Zeeman levels of the relevant D and Q states. The size of the ellipse on each spin level represents its population qualitatively.

by only ~0.35 T or $\sim 10^{-5}$ eV, which is negligible compared to the overall free energy change for charge separation $\Delta G(^*D \rightarrow D_1') \cong -0.8$ eV for **6**, Figure 2, producing a nonpolarized D_1'state (ignoring thermal polarization), which is analogous to the singlet RP produced in the model systems **4** and **7**. The Q_1 state is not populated initially as a result of spin conservation during the ultrafast charge separation. The D_1 state, which is energetically far removed from the $D_1'$and Q_1 states, does not mix with them at ~0.35 T, the field strength at which the TREPR spectra were measured.

The above reasoning is corroborated by the MFE and TREPR results for **6**, both of which probe the D_1'-Q_1 splitting, Δ_{DQ}, of the triradical state.[37] The TREPR spectra of $MeOAn^{+\bullet}$−6ANI−Ph(BPNO$^\bullet$)−$NI^{-\bullet}$ (Figure 7) are simulated with a two-state mixing model similar to the one outlined previously,[76] yielding $\Delta_{DQ} = 1.5$ mT, in agreement with the dominant value obtained from the MFE. The overall observed TREPR spectra are simulated by the sum of all the above "e" and "a" peaks weighted by the nuclear spin states, and the RP sign rule[76,77] indicates the sign of Δ_{DQ} from the polarization pattern of field-swept TREPR spectra

$$\Gamma = \mu \cdot \mathrm{sign}(\Delta_{DQ}) = \begin{cases} - & \text{e a} \\ + & \text{a e} \end{cases} \qquad (2)$$

where μ equals −1 or +1 for a doublet or a quartet precursor, the former being the case here. Therefore, the experimental e a pattern in Figure 7B confirms Δ_{DQ} to be positive, that is, D_1' higher in energy than Q_1.

Neutral Three-Spin States Formed upon Charge Recombination. Our earlier studies of **8**[38] as well as other closely related molecules[41,76,79] have shown that RP-ISC is followed by charge recombination, returning part of the population to the ground state, D_0, and the remainder to the local neutral triplet state, for example, MeOAn−6ANI−Ph(NN$^{\bullet}$)−^{3*}NI for **8**. Thus, charge recombination results in a neutral three-spin system that can be described by a new basis set of doublet and quartet states, labeled in Figure 10 as D_2 and Q_2. No spin flip occurs during charge recombination so that the Q_2 state inherits the population of the ±1/2 sublevels of Q_1 generated by RP-ISC from D_1'. However, the D_2 state becomes a mixture of the D_1' and D_1 states,[80] because charge recombination is accompanied by the rise of an extremely large same-site exchange interaction between the two unpaired spins of ^{3*}NI, which is estimated at 0.90 eV, the S_1-T_1 energy gap of NI.[79] D_0, D_2, and Q_2 form a complete spin basis set for the three-spin neutral states, which are different from the other set, D_1, D_1', and Q_1, that characterizes the three-spin RP state. Consequently, charge recombination from the triradical state requires switching or projection of the spin basis set. The charge recombination rates from the triradical state of **6** are related to k_{CRS} and k_{CRT} as shown in Figure 10. We have shown that the rate of charge recombination from the quartet triradical state Q_1 is the same as if the third spin does not exist:[39] $k_{CR}(Q_1 \rightarrow Q_2) = k_{CRT}$. In contrast, the total observed k_{CR} from the D_1'state turns into a weighted average of k_{CRS} and k_{CRT},

$$k_{CR}(D_1' \rightarrow D_0 + D_2) = 3/4\, k_{CRS} + 1/4\, k_{CRT} \qquad (3)$$

as compared to $k_{CR} = k_{CRS}$ for model compound **4**. This recombination rate is similar for the D_1 state and also qualitatively correct if an effective overall decay rate out of both D_1 and D_1' states is considered. Accordingly, overall charge recombination from the triradical state is accelerated if $k_{CRT} > k_{CRS}$ and otherwise slowed down. For **6**, in which ^{2,4}(MeOAn$^{+\bullet}$−6ANI−Ph(BPNO$^{\bullet}$)−NI$^{-\bullet}$) is in equilibrium with ^{2,4}(MeOAn−6ANI−Ph(BPNO$^{\bullet}$)−^{3*}NI), it has been shown for closely related molecules that the net k_{CRT} is slower than k_{CRS},[81,82] and thus, the lifetime of the photogenerated RP observed for **6** is extended by coupling to the third spin (Table 1), as determined here using both nanosecond transient absorption and TREPR.

In our earlier work on the photogenerated triradical ^{2,4}(MeOAn$^{+\bullet}$−6ANI−Ph(NN$^{\bullet}$)−NI$^{-\bullet}$) produced from **8**, we observed transfer of spin polarization from the mixed D_1'−Q_1 state of the triradical to the radical NN$^{\bullet}$. The overall spin polarization in **8** was attributed to nonadiabatic spin evolution driven by the spin−spin exchange interaction, as has been observed earlier in bacterial photosynthetic reactions centers.[83,84] Although RP-ISC processes in general do not generate a net overall spin polarization, the theory of chemically induced dynamic electron polarization[85] has been well established for doublet−doublet[74,78,86] and triplet−doublet[36,68,87−94] interactions. The difference between the magnetic environments of ^{3*}NI and BPNO$^{\bullet}$, although overcome by the exchange coupling between the two, contaminates and mixes the D_2 and Q_2 states. In particular, the ZFS term of triplets

$$H_{ZFS} = D\,(S_z^2 - {}^1/_3\,S^2) + E(S_x^2 - S_y^2) = D(S_z^2 - {}^1/_3 S^2) + {}^1/_2 E\,(S_+^2 + S_-^2) \quad (4)$$

contains the double-quantum terms S_+^2 and S_-^2 when the triplet is localized and E is significant. It is important to note that we do not observe spin polarization transfer from ^{2,4}(MeOAn−6ANI−Ph(BPNO$^{\bullet}$)−^{3*}NI) to BPNO$^{\bullet}$. This can be explained by the fact that the two ZFS terms, S_+^2 and S_-^2, in eq 4 do not couple the $|D_2 - 1/2\rangle$ sublevel, populated from D_1 and D_1'states, and the vacant $|Q_2 + 3/2\rangle$ sublevel due to their larger difference in energy in **6** relative to that in **8**.[88,89,95] This larger energy difference stems from the larger exchange interaction between ^{3*}NI and BPNO$^{\bullet}$ arising from the larger degree of spin delocalization into the Ph bridge in ^{2,4}(MeOAn−6ANI−Ph(BPNO$^{\bullet}$)−^{3*}NI).

Conclusions

We have demonstrated that the BPNO$^{\bullet}$ radical located on the Ph bridge of MeOAn−6ANI−Ph−NI influences the spin dynamics of the photogenerated RPs, resulting in the observation of two charge recombination pathways: a slow pathway involving 25% of the population and a fast pathway involving 75% of the population. Spin delocalization from BPNO$^{\bullet}$ to the Ph bridge increases the rate of RP-ISC by ∼100 times in the photogenerated triradical states MeOAn$^{+\bullet}$−6ANI−Ph(BPNO$^{\bullet}$)−NI$^{-\bullet}$, as compared to MeOAn$^{+\bullet}$−6ANI−Ph(NN$^{\bullet}$)−NI$^{-\bullet}$ and the corresponding two-spin system MeOAn$^{+\bullet}$−6ANI−Ph−NI$^{-\bullet}$. The increase in the rate of RP-ISC makes it possible to observe directly the rapid equilibrium that occurs between MeOAn$^{+\bullet}$−6ANI−Ph(BPNO$^{\bullet}$)−NI$^{-\bullet}$ and MeOAn−6ANI−Ph(BPNO$^{\bullet}$)−^{3*}NI. The triradical states and the neutral three-spin recombination products belong to different spin spaces, and charge recombination is accompanied by switching of the spin basis set. Spin polarization generated in the triradical state is carried over to the neutral three-spin recombination product. However, spin polarization is not transferred to the BPNO$^{\bullet}$ radical because the increased spin−spin exchange interaction between ^{3*}NI and BPNO$^{\bullet}$ arising from the larger degree of spin delocalization into the Ph bridge results in a larger doublet−quartet splitting. Thus, the degree of control over spin polarization transfer afforded by these tailored three-spin systems makes it possible to contemplate spintronic devices based on photocontrolled electron-transfer processes within multispin organic molecules.

Acknowledgment. The work was supported by the National Science Foundation under Grant No. CHE-0415730 and by DARPA. E.T.C. thanks the Natural Sciences and Engineering Research Council of Canada (NSERC). The Bruker E580 spectrometer was purchased with support in part from NSF Grant No. CHE-0131048.

Supporting Information Available: Synthesis and characterization details for all new compounds are available in the Supporting Information. This material is available free of charge via the Internet at http://pubs.acs.org.

References and Notes

(1) Wasielewski, M. R. *J. Org. Chem.* **2006**, *71*, 5051−5066.

(2) Benniston, A. C.; Harriman, A. *Chem. Soc. Rev.* **2006**, *35*, 169−179.

(3) Wasielewski, M. R. *Chem. Rev.* **1992**, *92*, 435−461.

(4) Gust, D.; Moore, T. A.; Moore, A. L. *Acc. Chem. Res.* **2001**, *34*, 40−48.

(5) Hush, N. S.; Paddon-Row, M. N.; Cotsaris, E.; Oevering, H.; Verhoeven, J. W.; Heppener, M. *Chem. Phys. Lett.* **1985**, *117*, 8−11.

(6) Oevering, H.; Paddon-Row, M. N.; Heppener, M.; Oliver, A. M.; Cotsaris, E.; Verhoeven, J. W.; Hush, N. S. *J. Am. Chem. Soc.* **1987**, *109*, 3258−3269.

(7) Paddon-Row, M. N.; Verhoeven, J. W. *New J. Chem.* **1991**, *15*, 107−116.

(8) Warman, J. M.; Smit, K. J.; Jonker, S. A.; Verhoeven, J. W.; Oevering, H.; Kroon, J.; Paddon-Row, M. N.; Oliver, A. M. *Chem. Phys.* **1993**, *170*, 359−380.
(9) Guldi, D. M.; Maggini, M.; Scorrano, G.; Prato, M. *J. Am. Chem. Soc.* **1997**, *119*, 974−980.
(10) Pullen, S. H.; Edington, M. D.; Studer-Martinez, S. L.; Simon, J. D.; Staab, H. A. *J. Phys. Chem. A* **1999**, *103*, 2740−2743.
(11) Newton, M. D. *Int. J. Quantum Chem.* **2000**, *77*, 255−263.
(12) Guldi, D. M.; Swartz, A.; Luo, C.; Gomez, R.; Segura, J. L.; Martin, N. *J. Am. Chem. Soc.* **2002**, *124*, 10875−10886.
(13) Napper, A. M.; Head, N. J.; Oliver, A. M.; Shephard, M. J.; Paddon-Row, M. N.; Read, I.; Waldeck, D. H. *J. Am. Chem. Soc.* **2002**, *124*, 10171−10181.
(14) Sutin, N.; Brunschwig, B. S.; Creutz, C. *J. Phys. Chem. B* **2003**, *107*, 10687−10690.
(15) Paddon-Row, M. N. *Aust. J. Chem.* **2003**, *56*, 729−748.
(16) Oosterbaan, W. D.; Koper, C.; Braam, T. W.; Hoogesteger, F. J.; Piet, J. J.; Jansen, B. A. J.; Van Walree, C. A.; Van Ramesdonk, H. J.; Goes, M.; Verhoeven, J. W.; Schuddeboom, W.; Warman, J. M.; Jenneskens, L. W. *J. Phys. Chem. A* **2003**, *107*, 3612−3624.
(17) Liu, M.; Waldeck, D. H.; Oliver, A. M.; Head, N. J.; Paddon-Row, M. N. *J. Am. Chem. Soc.* **2004**, *126*, 10778−10786.
(18) Sutin, N.; Brunschwig, B. S.; Creutz, C.; Feldberg, S. W. *J. Phys. Chem. B* **2004**, *108*, 12092−12102.
(19) Weiss, E. A.; Ahrens, M. J.; Sinks, L. E.; Gusev, A. V.; Ratner, M. A.; Wasielewski, M. R. *J. Am. Chem. Soc.* **2004**, *126*, 5577−5584.
(20) Weiss, E. A.; Tauber, M. J.; Kelley, R. F.; Ahrens, M. J.; Ratner, M. A.; Wasielewski, M. R. *J. Am. Chem. Soc.* **2005**, *127*, 11842−11850.
(21) Dance, Z. E. X.; Mi, Q.; McCamant, D. W.; Ahrens, M. J.; Ratner, M. A.; Wasielewski, M. R. *J. Phys. Chem. B* **2006**, *110*, 25163−25173.
(22) Ljungdahl, T.; Pettersson, K.; Albinsson, B.; Martensson, J. *Eur. J. Org. Chem.* **2006**, 3087−3096.
(23) Eng, M. P.; Ljungdahl, T.; Mrtensson, J.; Albinsson, B. *J. Phys. Chem. B* **2006**, *110*, 6483−6491.
(24) Pettersson, K.; Wiberg, J.; Ljungdahl, T.; Mrtensson, J.; Albinsson, B. *J. Phys. Chem. A* **2006**, *110*, 319−326.
(25) Prisner, T.; Dobbert, O.; Dinse, K. P.; van Willigen, H. *J. Am. Chem. Soc.* **1988**, *110*, 1622−1623.
(26) Angerhofer, A.; Toporowicz, M.; Bowman, M. K.; Norris, J. R.; Levanon, H. *J. Phys. Chem.* **1988**, *92*, 7164−7166.
(27) Hayashi, H. *Introduction to Dynamic Spin Chemistry: Magnetic Field Effects upon Chemical and Biochemical Reactions*; World Scientific: Singapore, 2004.
(28) Buchachenko, A. L.; Ruban, L. V.; Step, E. N.; Turro, N. J. *Chem. Phys. Lett.* **1995**, *233*, 315−318.
(29) Vlassiouk, I.; Smirnov, S.; Kutzki, O.; Wedel, M.; Montforts, F. P. *J. Phys. Chem. B* **2002**, *1*−*6*, 8657−8666.
(30) Smirnov, S.; Vlassiouk, I.; Kutzki, O.; Wedel, M.; Montforts, F. P. *J. Am. Chem. Soc.* **2002**, *124*, 4212−4213.
(31) Buchachenko, A. L.; Berdinsky, V. L. *Chem. Rev.* **2002**, *102*, 603−612.
(32) Volkova, O. S.; Taraban, M. B.; Plyusnin, V. F.; Leshina, T. V.; Egorov, M. P.; Nefedov, O. M. *J. Phys. Chem. A* **2003**, *107*, 4001−4005.
(33) Mori, Y.; Sakaguchi, Y.; Hayashi, H. *J. Phys. Chem. A* **2002**, *106*, 4453−4467.
(34) Mori, Y.; Sakaguchi, Y.; Hayashi, H. *Bull. Chem. Soc. Jpn.* **2001**, *74*, 293−304.
(35) Ishii, K.; Hirose, Y.; Kobayashi, N. *J. Phys. Chem. A* **1999**, *103*, 1986−1990.
(36) Ishii, K.; Hirose, Y.; Fujitsuka, H.; Ito, O.; Kobayashi, N. *J. Am. Chem. Soc.* **2001**, *123*, 702−708.
(37) Weiss, E. A.; Chernick, E. T.; Wasielewski, M. R. *J. Am. Chem. Soc.* **2004**, *126*, 2326−2327.
(38) Chernick, E. T.; Mi, Q.; Kelley, R. F.; Weiss, E. A.; Jones, B. A.; Marks, T. J.; Ratner, M. A.; Wasielewski, M. R. *J. Am. Chem. Soc.* **2006**, *128*, 4356−4364.
(39) Mi, Q.; Chernick, E. T.; McCamant, D. W.; Weiss, E. A.; Ratner, M. A.; Wasielewski, M. R. *J. Phys. Chem. A* **2006**, *110*, 7323−7333.
(40) Davis, M. S.; Kreilick, R. W.; Morokuma, K. *J. Am. Chem. Soc.* **1972**, *94*, 5588−5592.
(41) Lukas, A. S.; Bushard, P. J.; Weiss, E. A.; Wasielewski, M. R. *J. Am. Chem. Soc.* **2003**, *125*, 3921−3930.
(42) Shaakov, S.; Galili, T.; Stavitski, E.; Levanon, H.; Lukas, A.; Wasielewski, M. R. *J. Am. Chem. Soc.* **2003**, *125*, 6563−6572.
(43) Shultz, D. A.; Gwaltney, K. P.; Lee, H. *J. Org. Chem.* **1998**, *63*, 769−774.
(44) Iida, T.; Ohshita, J.; Uemura, T.; Fukuoka, H.; Ohta, N.; Komaguchi, K.; Itagaki, Y.; Shiotani, M.; Yamanaka, S.; Kunai, A. *Silicon Chem.* **2002**, 383−389.
(45) Giaimo, J. M.; Gusev, A. V.; Wasielewski, M. R. *J. Am. Chem. Soc.* **2002**, *124*, 8530−8531.
(46) Schweiger, A.; Jeschke, G. *Principles of pulsed electron paramagnetic resonance*; Oxford: Oxford, 2001.
(47) Greenfield, S. R.; Svec, W. A.; Gosztola, D.; Wasielewski, M. R. *J. Am. Chem. Soc.* **1996**, *118*, 6767−6777.
(48) Debreczeny, M. P.; Svec, W. A.; Marsh, E. M.; Wasielewski, M. R. *J. Am. Chem. Soc.* **1996**, *118*, 8174−8175.
(49) Suga, T.; Pu, Y. J.; Oyaizu, K.; Nishide, H. *Bull. Chem. Soc. Jpn.* **2004**, *77*, 2203−2204.
(50) Kobori, Y.; Sekiguchi, S.; Akiyama, K.; Tero-Kubota, S. *J. Phys. Chem. A* **1999**, *103*, 5416−5424.
(51) Paddon-Row, M. N.; Shephard, M. J. *J. Phys. Chem. A* **2002**, *106*, 2935−2944.
(52) Volk, M.; Haberle, T.; Feick, R.; Ogrodnik, A.; Michel-Beyerle, M. E. *J. Phys. Chem.* **1993**, *97*, 9831−9836.
(53) Weller, A.; Staerk, H.; Treichel, R. *Faraday Discuss. Chem. Soc.* **1984**, *78*, 271−278.
(54) Hoff, A. J.; Gast, P.; van der Vos, R.; Franken, E. M.; Lous, E. J. *Z. Phys. Chem.* **1993**, *180*, 175−192.
(55) Till, U.; Hore, P. J. *Mol. Phys.* **1997**, *90*, 289−296.
(56) Steiner, U. E.; Ulrich, T. *Chem. Rev.* **1989**, *89*, 51−147.
(57) Schulten, K.; Staerk, H.; Weller, A.; Werner, H. J.; Nickel, B. *Z. Phys. Chem.* **1976**, *101*, 371−390.
(58) Tanimoto, Y.; Okada, N.; Itoh, M.; Iwai, K.; Sugioka, K.; Takemura, F.; Nakagaki, R.; Nagakura, S. *Chem. Phys. Lett.* **1987**, *136*, 42−46.
(59) Sakaguchi, Y.; Hayashi, H. *J. Phys. Chem. A* **1997**, *101*, 549−555.
(60) Werner, U.; Kuhnle, W.; Staerk, H. *J. Phys. Chem.* **1993**, *97*, 9280−9287.
(61) Weiss, E. A.; Ratner, M. A.; Wasielewski, M. R. *J. Phys. Chem. A* **2003**, *107*, 3639−3647.
(62) Tadjikov, B.; Smirnov, S. *Phys. Chem. Chem. Phys.* **2001**, *3*, 204−212.
(63) Tsentalovich, Y. P.; Morozova, O. B.; Avdievich, N. I.; Ananchenko, G. S.; Yurkovskaya, A. V.; Ball, J. D.; Forbes, M. D. E. *J. Phys. Chem. A* **1997**, *101*, 8809−8816.
(64) Blankenship, R. E.; Schaafsma, T. J.; Parson, W. W. *Biochim. Biophys. Acta* **1977**, *461*, 297−305.
(65) Plato, M.; Möbius, K.; Michel-Beyerle, M. E.; Bixon, M.; Jortner, J. *J. Am. Chem. Soc.* **1988**, *110*, 7279−7285.
(66) Werner, H.-J.; Schulten, K.; Weller, A. *Biochim. Biophys. Acta* **1978**, *502*, 255−268.
(67) Norris, J. R.; Bowman, M. K.; Budil, D. E.; Tang, J.; Wraight, C. A.; Closs, G. L. *Proc. Natl. Acad. Sci. U.S.A.* **1982**, *79*, 5532−5536.
(68) Yamauchi, S. *Bull. Chem. Soc. Jpn.* **2004**, *77*, 1255−1268.
(69) Haberkorn, R.; Michel-Beyerle, M. E. *Biophys. J.* **1979**, *26*, 489−498.
(70) Hoff, A. J.; Rademaker, H.; Van Grondelle, R.; Duysens, L. N. M. *Biochim. Biophys. Acta* **1977**, *460*, 547−554.
(71) Mori, Y.; Sakaguchi, Y.; Hayashi, H. *J. Phys. Chem. A* **2000**, *104*, 4896−4905.
(72) Wegner, M.; Fischer, H.; Grosse, S.; Vieth, H. M.; Oliver, A. M.; Paddon-Row, M. N. *Chem. Phys.* **2001**, *264*, 341.
(73) Hasharoni, K.; Levanon, H.; Greenfield, S. R.; Gosztola, D. J.; Svec, W. A.; Wasielewski, M. R. *J. Am. Chem. Soc.* **1995**, *117*, 8055−8056.
(74) Closs, G. L.; Forbes, M. D. E.; Norris, J. R. *J. Phys. Chem.* **1987**, *91*, 3592−3599.
(75) Kobori, Y.; Kawai, A.; Obi, K. *J. Phys. Chem.* **1994**, *98*, 6425−6429.
(76) Shaakov, S.; Galili, T.; Stavitski, E.; Levanon, H.; Lukas, A. S.; Wasielewski, M. R. *J. Am. Chem. Soc.* **2003**, *125*, 6563−6572.
(77) Hasharoni, K.; Levanon, H.; Greenfield, S. R.; Gosztola, D. J.; Svec, W. A.; Wasielewski, M. R. *J. Am. Chem. Soc.* **1996**, *118*, 10228−10235.
(78) McLauchlan, K. A. In *Modern pulsed and continuous-wave electron spin resonance*; Kevan, L., Bowman, M. K., Eds.; Wiley: New York, 1990, pp 285−363.
(79) Wiederrecht, G. P.; Svec, W. A.; Wasielewski, M. R.; Galili, T.; Levanon, H. *J. Am. Chem. Soc.* **2000**, *122*, 9715−9722.
(80) Hoytink, G. J. *Acc. Chem. Res.* **1969**, *2*, 114−120.
(81) Weiss, E. A.; Tauber, M. J.; Ratner, M. A.; Wasielewski, M. R. *J. Am. Chem. Soc.* **2005**, *127*, 6052−6061.
(82) Weiss, E. A.; Sinks, L. E.; Lukas, A. S.; Chernick, E. T.; Ratner, M. A.; Wasielewski, M. R. *J. Phys. Chem. B* **2004**, *108*, 10309−10316.
(83) Hoff, A. J.; Gast, P. *J. Phys. Chem.* **1979**, *83*, 3355−3358.
(84) Gast, P.; Hoff, A. J. *Biochim. Biophys. Acta* **1979**, *548*, 520−535.
(85) Muus, L. T.; Atkins, P. W.; McLauchlan, K. A.; Pedersen, J. B. *Chemically induced magnetic polarization*; Reidel: Dordrecht, Boston, 1977.
(86) Norris, J. R.; Morris, A. L.; Thurnauer, M. C.; Tang, J. *J. Chem. Phys.* **1990**, *92*, 4239−4249.
(87) Blattler, C.; Jent, F.; Paul, H. *Chem. Phys. Lett.* **1990**, *166*, 375−380.
(88) Kawai, A.; Okutsu, T.; Obi, K. *J. Phys. Chem.* **1991**, *95*, 9130−9134.
(89) Goudsmit, G. H.; Paul, H.; Shushin, A. I. *J. Phys. Chem.* **1993**, *97*, 13243−13249.

(90) Corvaja, C.; Maggini, M.; Prato, M.; Scorrano, G.; Venzin, M. *J. Am. Chem. Soc.* **1995**, *117*, 8857−8858.
(91) Ishii, K.; Fujisawa, J.; Ohba, Y.; Yamauchi, S. *J. Am. Chem. Soc.* **1996**, *118*, 13079−13080.
(92) Fujisawa, J.; Ishii, K.; Ohba, Y.; Yamauchi, S.; Fuhs, M.; Möbius, K. *J. Phys. Chem. A* **1999**, *103*, 213−216.
(93) Blank, A.; Levanon, H. *J. Phys. Chem. A* **2001**, *105*, 4799−4807.
(94) Conti, F.; Corvaja, C.; Maggini, M.; Scorrano, G.; Ceroni, P.; Paolucci, F.; Roffia, S. *Phys. Chem. Chem. Phys.* **2001**, *3*, 3518−3525.
(95) Kobori, Y.; Takeda, K.; Tsuji, K.; Kawai, A.; Obi, K. *J. Phys. Chem. A* **1998**, *102*, 5160−5170.